Commun. Comput. Phys.
doi: 10.4208/cicp.170512.310113a

Vol. **14**, No. 4, pp. 979-1000
October 2013

Multiscale Finite Element Methods for Flows on Rough Surfaces

Yalchin Efendiev[1], Juan Galvis[2,*] and M. Sebastian Pauletti[1]

[1] *Department of Mathematics, TAMU, College Station, TX 77843-3368, USA.*
[2] *Departamento de Matemáticas, Universidad Nacional de Colombia, Bogotá, Colombia.*

Received 17 May 2012; Accepted (in revised version) 31 January 2013

Available online 18 April 2013

Abstract. In this paper, we present the Multiscale Finite Element Method (MsFEM) for problems on rough heterogeneous surfaces. We consider the diffusion equation on oscillatory surfaces. Our objective is to represent small-scale features of the solution via multiscale basis functions described on a coarse grid. This problem arises in many applications where processes occur on surfaces or thin layers. We present a unified multiscale finite element framework that entails the use of transformations that map the reference surface to the deformed surface. The main ingredients of MsFEM are (1) the construction of multiscale basis functions and (2) a global coupling of these basis functions. For the construction of multiscale basis functions, our approach uses the transformation of the reference surface to a deformed surface. On the deformed surface, multiscale basis functions are defined where reduced (1D) problems are solved along the edges of coarse-grid blocks to calculate nodal multiscale basis functions. Furthermore, these basis functions are transformed back to the reference configuration. We discuss the use of appropriate transformation operators that improve the accuracy of the method. The method has an optimal convergence if the transformed surface is smooth and the image of the coarse partition in the reference configuration forms a quasiuniform partition. In this paper, we consider such transformations based on harmonic coordinates (following H. Owhadi and L. Zhang [Comm. Pure and Applied Math., LX(2007), pp. 675–723]) and discuss gridding issues in the reference configuration. Numerical results are presented where we compare the MsFEM when two types of deformations are used for multiscale basis construction. The first deformation employs local information and the second deformation employs a global information. Our numerical results show that one can improve the accuracy of the simulations when a global information is used.

AMS subject classifications: 65N30, 58E20,76M50, 37E35

Key words: Multiscale finite elements on surfaces, Laplace Beltrami, resonance error, harmonic maps.

*Corresponding author. *Email addresses:* efendiev@math.tamu.edu (Y. Efendiev), jcgalvisa@unal.edu.co (J. Galvis), pauletti@math.tamu.edu (M. S. Pauletti)

1 Introduction

Complex processes on rough surfaces occur in many applications. These include surface processes, such as diffusion on a rough terrains, or volume processes in geometrically complicated 3D thin regions. In addition, complex processes on rough surfaces can happen when the dominant heterogeneities form complex geometrical shapes. For example, if we consider the diffusion process in a heterogeneous media (i.e., coefficients representing conductivity are highly variable), then the diffusion in high-conductivity regions is a dominant factor that determines the outcome of these processes. One can write the diffusion equation restricted to the high conductivity region and approximate the resulting model by a diffusion equation on a rough surface. In summary, the small scales inherent to applications of diffusion problems on surfaces are caused by the presence of

- highly oscillatory geometrical properties;
- highly oscillatory conductivity coefficients.

Because of high spatial resolutions of these rough surfaces, the detailed simulations of complex processes can be prohibitively expensive. For this reason, some type of coarsening or upscaling is needed (see [3,39]). In these approaches, oscillatory geometric properties are represented on a coarse grid by local shape functions. These local shape functions are further coupled to solve the underlying problem on a coarse grid with a reduced computational cost. In this paper, we propose a new class of MsFEMs where the underlying fine-scale local problems are solved on a heterogeneous surface directly. In particular, we consider the problem of approximating the solution of the equation

$$-\mathrm{div}_s(\kappa\nabla_s u) = f \text{ in } \Gamma \quad \text{and} \quad u = g \text{ on } \partial\Gamma, \tag{1.1}$$

where ∇_s and div_s denote the surface gradient and the surface divergence, respectively.

In this paper, we construct Multiscale Finite Element Methods (MsFEMs) to approximate equation (1.1). We note that, MsFEMs are suited to obtain inexpensive approximations of problems with underlying complicated multiscale structures. MsFEMs consist of two major ingredients: (1) a small number of multiscale basis functions and (2) a global numerical formulation which couples these multiscale basis functions. Multiscale basis functions are designed to capture the effects on the solution caused by small scale parameters such as small scale geometrical variations of the domain where the problem is posed. In general, important small scale features of the solution need to be incorporated into these localized basis functions which contain information about the scales which are smaller (as well as larger) than the local numerical scale defined by the basis functions. In this paper, we study MsFEM approximation of multiscale elliptic problems on oscillatory surfaces.

We present a unified framework for MsFEMs that depends on a general coordinate transformation which deforms the reference surface and it is used to compute multiscale basis functions. This is motivated by the work of Owhadi and Zhang and suits well to

the framework of problems on rough surfaces; see [42]. In this framework, we introduce a mapping of the rough surface, where the problem is posed, to another surface which is possibly smoother (and it presents less roughness than the original surface or no roughness at all). Using these coordinate transformations, one can define boundary conditions for multiscale basis functions. In particular, boundary conditions for multiscale functions are constructed as the solution of the reduced problem along the boundaries of the coarse element on the deformed surface. These are nodal basis functions and, once their values at the vertices are defined, the reduced one-dimensional problem along the edge is well posed. Other standard constructions of appropriate boundary conditions can be also used on the deformed surface. Furthermore, these boundary conditions are mapped back to the reference surface which gives the boundary conditions for multiscale basis functions in the reference configuration. Once boundary conditions are computed, multiscale basis functions are defined as the solution of local problems in each coarse region. If boundary conditions are chosen properly, MsFEM converges independent of small scale (i.e., there are no resonance errors). In this sense, the correct choice of boundary condition is dictated on the deformed surface. The correct choice of boundary conditions depends mainly on two aspects: 1) the resulting equation after the change of coordinates and 2) the coarse grid employed in the deformed surface. Thus, our goal is to achieve a smoothly deformed surface and a regular partition on deformed surface in order to guarantee that MsFEM converges independent of small scales. In this paper, we discuss these issues and show that appropriate domain transformation can help to reduce the error substantially.

In a previous work [3], the authors designed multiscale solution techniques using Heterogeneous Multiscale Method (HMM). In this construction, local problems in representative volume are solved to construct a coarse-grid approximation of the solution. Though MsFEM and HMM share many similarities, there are some differences (see [25] for details). In particular, the approaches designed here are intended for problems without scale separation. We also plan to use the proposed methods to construct efficient solvers for problems with both small scales and high contrast ([20–22]). As we have shown in [20–22], multiscale basis functions such as those constructed here are crucial for efficient solvers. We would also like to mention that there are investigations where the domain has oscillations near or along the (exterior) boundaries (see [39]). In these approaches, multiscale basis functions are constructed for coarse elements near the boundaries where the oscillation is present.

In our numerical tests, we consider various rough surfaces that are obtained by perturbing a planar surface, a sphere and a torus. These surfaces are perturbed by quasi-periodic functions. As we noted earlier, these perturbations do not result to periodic problems that can be solved using a period as a representative element. We present in detail two main coordinate transformation choices. Our first choice is the identity which results to boundary conditions constructed by solving a reduced problem on the boundary. More precisely, the boundary condition solves a local one-dimensional problem along the rough edges of the boundary of coarse regions. Our second choice is the use of harmonic-like coordinates. The new coordinates are constructed using the solution

of a (vector-valued) Laplace-Beltrami equation. In this case, the boundary conditions are constructed by solving reduced problems along the edges in the new coordinates. We show that the second choice provides much better accuracy compared to the first approach. This fact is known for problems posed in two dimensional domains if the coarse grid in the original (or transformed) domain is chosen properly; see [42]. For problems posed in two dimensional domains, when the coarse grid in the transformed domain satisfies requirements that guarantee good approximation in finite element methods, we observe a standard convergence for MsFEM in the original domain. In general, one has to select oscillatory coarse grids in the reference configuration that are obtained from a regular coarse grid in the deformed configuration. The computational construction of such adequate grids is more involved for the cases where the transform surface is not a planar surface. We discuss these issues. We also briefly discuss how one can enrich coarse spaces as an alternative approach to avoid the construction of complicated grids.

The paper is organized as follows. In the next section, we describe diffusion on rough surfaces and introduce some preliminary notations. In Section 3, we discuss the general framework for MsFEM. Section 4 is devoted to the construction of coarse spaces that are used in MsFEM. Finally, we present numerical results in Section 5.

2 Description of problems on rough surfaces

Let Γ be an orientable compact smooth 2-dimensional surface embedded in $\mathbb{R}^3$ with boundary. Let $\boldsymbol{\nu}:\Gamma\to\mathbb{R}^3$ be the unit normal given by the orientation. Our goal is to construct numerical approximations of the elliptic equation

$$-\mathrm{div}_s(\kappa\nabla_s u)=f \ \text{ in } \Gamma \quad \text{ and } \quad u=g \ \text{ on } \partial\Gamma, \tag{2.1}$$

where ∇_s and div_s denote the surface gradient and the surface divergence, respectively, and (for later use) Δ_s denotes the Laplace-Beltrami operator. These differential operators can be equivalently defined by either using function extensions to an ambient neighborhood of Γ and Euclidean differential calculus in the neighborhood [14, 29, 44] or through local parametrization [15]. In the latter case, if $\boldsymbol{X}:\Omega\to\Gamma$ is a local parametrization and u is a scalar function defined on Γ, then $\nabla_s u=D\boldsymbol{X}G^{-1}\nabla\hat{u}$, where $G=D\boldsymbol{X}^*D\boldsymbol{X}$, $\hat{u}=u\circ\boldsymbol{X}$ and $D\boldsymbol{X}$ is the derivative of $\boldsymbol{X}$. The quantity $\nabla_s u$ is independent of the parametrization.

The *second fundamental form* is $\nabla_s\boldsymbol{\nu}$. This symmetric tensor has the eigenvector $\boldsymbol{\nu}$ with zero eigenvalue. The remaining eigenvalues are the *principal curvatures*. In local coordinates this curvature tensor is given by $\boldsymbol{G}^{-1}\boldsymbol{B}$, where $b_{ij}=<\boldsymbol{\nu},\partial_{ij}\boldsymbol{X}>$ and ∂_{ij} denotes second derivatives.

To obtain a weak formulation of equation (1.1), we use Sobolev spaces on surfaces. Let $H^l(\Gamma)$ be the square integrable functions in $L^2(\Gamma)$ with weak tangential derivatives up to order l in $L^2(\Gamma)$. The Sobolev norms are defined in the usual way and $H_0^l(\Gamma)$ is the completion of $C_0^l(\Gamma)$ with the H^l-norm. We recall that, in order for the definition of $H^l(\Gamma)$

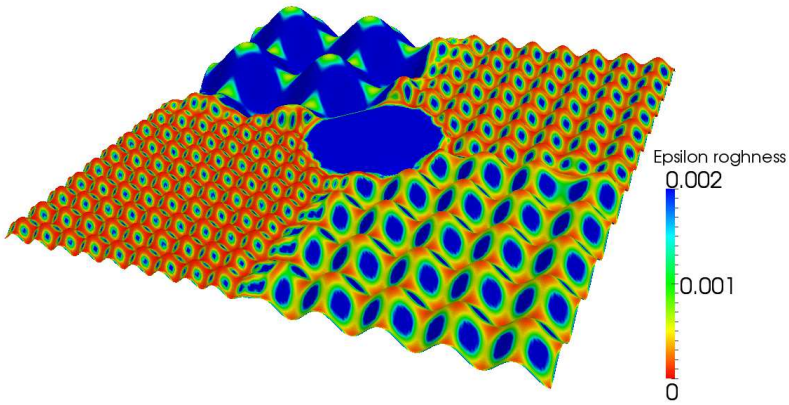

Figure 1: Oscillating surface constructed by blending together five different distinctive periodic roughnesses. The central region is flat and each corner of the square generates a local region of different roughnesses. In color we see the measure of the ϵ-roughness. The values of ϵ vary from 0 (red) to 0.0002 (blue). The smaller epsilon indicates the more roughness, whereas the larger epsilon indicates more smoothness.

to make sense, it is necessary that Γ is $C^{k,\alpha}$ with $k+\alpha \geq 1$ and $l \leq k+\alpha$ if $k+\alpha$ is a natural number and with strict inequality otherwise. For details the reader is referred to [4, 45].

After multiplying both sides of equation (1.1) by a smooth test function v vanishing on $\partial\Gamma$ and integrating by parts, we obtain the weak form of (2.1) which is to find $u \in H^1(\Gamma)$ with $u = g$ on $\partial\Gamma$ and such that

$$\int_\Gamma \nabla_s v \cdot \kappa \nabla_s u = \int_\Gamma f v \qquad \text{for all } v \in H_0^1(\Gamma). \tag{2.2}$$

Usual existence and regularity results hold for this problem; see [4] p.104.

Our goal is to approximate equation (2.2) using multiscale basis functions. We want to construct multiscale basis functions that represent the roughness of the surface in the sense that these basis capture the effect of the roughness of the surface on the solution of (2.2). Before discussing further about the basis functions, we take a time to describe the idea of roughness of a surface. Intuitively, we can characterize the geometric "roughness" of a surface in terms of its curvature. To make compatible the multiscale idea of an ϵ-rough coefficient (whose features are of scale ϵ) with the geometric idea of an ϵ-rough surface, we say that a surface Γ is ϵ-rough in a given region if for the points $\boldsymbol{p}$ in this region the quantity $\frac{\text{Area}(\Gamma)}{|\nabla_S \boldsymbol{\nu}(\boldsymbol{p})|^2}$ is bounded from below by ϵ. The smaller the ϵ the rougher the surface and vice-versa. For example, in Fig. 1 we show the roughness, i.e., the quantity $\frac{\text{Area}(\Gamma)}{|\nabla_S \boldsymbol{\nu}(\boldsymbol{p})|^2}$, on a surface with regions of distinctive geometric scales.

In this paper, we also assume that the conductivity coefficient κ does not affect the local behavior of the solution in the sense that multiscale basis functions constructed for the Laplace-Beltrami operator, are also effective for equation (2.2). The general case of constructing efficient numerical methods in the presence of (possible uncorrelated) oscillations in the geometry and the media properties is a topic of future research.

3 Multiscale finite element methods on surfaces

3.1 Finite element for surfaces

Before describing the MsFEM approximation on surfaces, we briefly describe a classical (fine scale) finite element approximation of elliptic problems on surfaces. This method was first proposed for the Laplace-Beltrami equation in [18].

We assume that the surface Γ can be approximated by polyhedral triangulations where we can define finite element spaces to approximate the continuous spaces. More precisely, we work on polyhedral surfaces. Let $h>0$. A pair $(\Gamma^h,\mathcal{T}^h)$ is a polyhedral surface if $\Gamma_h\subset\mathbb{R}^3$ and $\mathcal{T}_h$ is a finite family of closed, non degenerate, cells in $\mathbb{R}^3$ (triangles or quadrilaterals for two dimensional surfaces) such that the intersection of two cells in the family is either empty or a $(2-k)$-dimensional sub-cell of both cells $1\leq k<2$.

We denote the fine-grid cells by K_i^h, $i=1,\cdots,N_t^f$, the edges by e_i^h, $i=1,\cdots,N_e^f$, and vertex points by p_i^h, $i=1,\cdots,N_p^f$.

Equation (2.2) can be discretized using low-order continuous parametric finite elements following [18]. Let $\hat{K}\subset\mathbb{R}^d$ be the master cell. Given a cell K^h in $\mathbb{R}^3$, let $\boldsymbol{F}_K^h:\hat{K}\to K^h$ be an injective affine-linear (bilinear) map such that the vertices of $\hat{K}$ are mapped onto the vertices of K^h. A C^0-finite element space on the polyhedral surface Γ_h can then be defined as follows:

$$\mathbb{V}^h(\Gamma^h)=\{\Phi\in C^0(\Gamma^h):\Phi\circ\boldsymbol{F}_{K^h}\in\mathrm{P}(\hat{K})\quad\text{for all } K^h\in\mathcal{T}^h\},\tag{3.1}$$

where $\mathrm{P}(\hat{K})$ is the space of linear (bilinear) functions on $\hat{K}$.

The discrete version of (2.2) is: find $u^h\in\mathbb{V}(\Gamma^h)$ such that

$$a^h(u^h,v^h)=f^h(v^h),\quad\text{for all } v^h\in\mathbb{V}(\Gamma^h),\tag{3.2}$$

where

$$a^h(u,v)=\int_{\Gamma^h}\nabla_s v\cdot\kappa\nabla_s u=\sum_{K^h}\int_{K^h}\nabla_s v\cdot\kappa\nabla_s u\quad\text{for all } u,v\in\mathbb{V}(\Gamma^h)\tag{3.3}$$

and

$$f^h(v)=\int_{\Gamma^h}\tilde{f}v=\sum_{K^h}\int_{K^h}\tilde{f}v\quad\text{for all } v\in\mathbb{V}(\Gamma^h),$$

with $\tilde{f}$ being some projection of f from Γ to Γ^h. A simple application of the usual Hilbert space method shows existence and uniqueness of the discrete problem. The problem above is equivalent to the solution of a linear system

$$A^h u=b^h,\tag{3.4}$$

where the matrix $A^h=[a_{ij}^h]$ and the vector $b^h=[b_j^h]$ are defined by

$$u^T A^h v=a^h(u,v)\tag{3.5}$$

and $v^T b^h = f^h(v)$, respectively. Here and from now on, we use the same notation for finite element functions and their vectors of coordinates in the usual basis of the space of C^0-finite element functions.

The formulation (3.4) (or (3.2)) is our fine-scale (fine-grid) formulation and we assume that this fine resolution is smaller than the length scales associated with surface oscillations, i.e., $h<\epsilon$. Essentially, we are assuming that, at the fine resolution, we can describe all coefficients and geometrical oscillations accurately. We mention that it is typically prohibitively expensive to compute approximations of solutions at these fine resolutions. This is especially true for applications that require solving (3.4) many times for different right-hand sides.

It is also important to mention [18] that the usual error estimates $|u-u_h|_k \leq ch^{2-k}$ with $k=0,1$, hold in this case. With c depending linearly on the curvature (geometric dependence) and also linearly on the quotient between the maximum and minimum eigenvalue of κ (contrast dependence).

3.2 Coarse-grid definitions

As before, we are given a fine-grid triangulation (and recall that we denote the fine-grid cells by K_i^h, $i=1,\cdots,N_t^f$, the edges by e_i^h, $i=1,\cdots,N_e^f$, and vertex points by p_i^h, $i=1,\cdots,N_p^f$). Here and below, we consider the triangulation elements as closed sets (relatively to the surface).

In this section, we assume that a coarse triangulation is given. More precisely, we assume that we can use an agglomeration algorithm to obtain coarse-grid elements, coarse edges and coarse vertices that satisfy the usual requirements of admissible triangulations. We require a coarse-grid partition where

- each coarse-grid element K_I^H is a simply connected domain and it is a union of fine-grid elements, i.e., $K_I^H=\bigcup_{i\in S_{i,t}} K_i^h$, where $S_{i,e}$ is a subset of $\{1,\cdots,N_t^f\}$, $I=1,\cdots,N_t^c$;
- each coarse edge is a simply connected union of fine-grid edges, i.e., $e_I^H=\bigcup_{i\in S_{i,e}} e_i^h$, where $S_{i,e}$ is a subset of $\{1,\cdots,N_e^f\}$, $I=1,\cdots,N_e^c$;
- each coarse vertex p_I^H corresponds to some fine vertex;
- the following relations between coarse elements, coarse edges and coarse vertices hold:

    1. the intersection of two different coarse-grid elements is either empty, a coarse vertex or a whole coarse edge;
    2. the boundary of each coarse-grid element is a union of coarse edges;
    3. the intersection of two different coarse edges is either empty or a coarse vertex;
    4. the boundary of each coarse edge is the union of coarse vertices.

For each coarse vertex, p_I^H, we denote by ω_I the coarse-grid neighborhood of p_I^H that is defined by

$$\omega_I = \bigcup \{K_J^H \in \mathcal{P}^H; \quad p_I^H \in \overline{K}_J\}. \tag{3.6}$$

See Fig. 4 for an illustrative example.

The coarse discretization size H may be too coarse, in the sense that a polyhedral surface with representative size H, say Γ^H, does not describe accurately all the oscillations of the geometry and variations of the coefficients that occur at scale ϵ. We use MsFEM methods that use inexpensive global formulations and still capture fine grid effects accurately.

Remark 3.1 (Extension beyond surfaces)**.** All the methods and results of this paper could be, in principle, extended to other dimensions. For example, curves in the plane or space, open sets or even higher dimensional manifolds. We do not pursue this extension here for the following reasons:

- Problems on surfaces are by far the most useful case for applications.
- Working with surfaces allows us to use simpler notation and to make a better presentation of the method in terms of readability.

3.3 Global coupling of MsFEM on surfaces

We construct multiscale basis functions for each coarse node y_I. We denote the basis functions for the node p_I^H, χ_I, and assume that the basis functions are supported in ω_I. As in standard finite element methods, once multiscale basis functions are constructed (see Figs. 2 and 3 for the illustration), we seek $u_0 = \sum_I c_I \chi_I$, the Galerkin projection into the coarse subspace

$$V_0 = \text{span}\{\chi_I\}.$$

More precisely, we seek $u_0 \in V_0$ such that

$$a^h(u_0, v) = f^h(v), \quad \text{for all } v \in V_0. \tag{3.7}$$

The system above, determines the coordinates of u_0 with respect to the basis functions. Once c_i's are determined, one can define a fine-scale approximation of the solution by reconstructing via basis functions, $u_0 = \sum_i c_i \chi_i$. To write the matrix form of (3.7), we assume that the basis functions are defined on a fine grid and each basis χ_I has vector representation Φ_I, $I = 1, \cdots, N_c$, where N_c is the number of basis functions. Given these coarse-scale basis functions, the coarse matrix is given by

$$A_0 = R_0 A R_0^T,$$

where A is defined in (3.5) and $R_0^T = [\Phi_1, \cdots, \Phi_{N_c}]$. Here, Φ_i's are discrete coarse-scale basis functions defined on a fine grid (i.e., vectors). The coarse problem (3.7) is equivalent to the coarse linear system

$$A_0 c_0 = f_0,$$

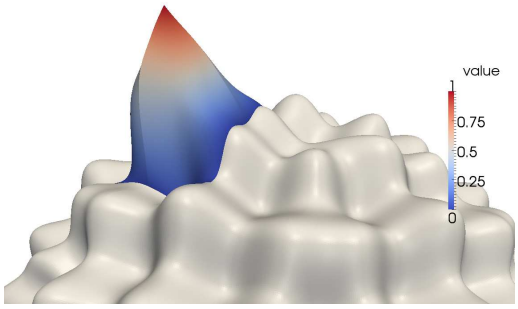

Figure 2: Illustration of a multiscale basis function defined over an oscillatory surface. The graph shows the basis function plotted on top of the surface in the direction of its normal vector.

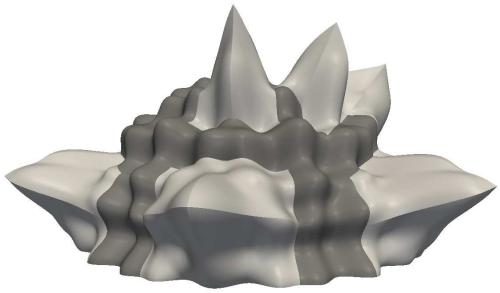

Figure 3: Illustration of some multiscale basis functions. Here we have included a few of the basis function for the same surface shown in Fig. 2 shows.

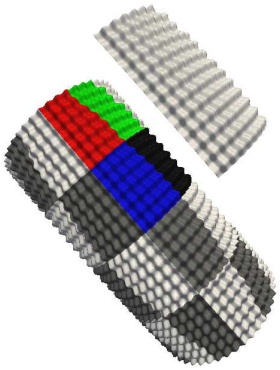

Figure 4: Schematic description of coarse regions. The figure shows an oscillatory surface constructed over a toroidal region. The light and dark regions show different coarse blocks. The four coarse blocks with a common vertex that are colored by red, green, blue, and black, constitute the support of the basis function χ_I, where p_I^H is the vertex where the blocks intersect.

where $f_0^h = R_0^T b$ and c_0 denotes the vector of coordinates of the solution of the coarse problem (3.7), $u_0 \in \mathbb{V}^h(\Gamma^h)$.

4 Coarse spaces

In this section, we discuss some coarse spaces constructed to capture the fine-scale features of the solution. We first introduce a transformation of the original surface to a modified surface where boundary conditions of basis functions are constructed and mapped back to the original surface. First, we assume this transformation is given and describe our multiscale methods. Then, we discuss how an appropriate choice of the transformation can improve the accuracy of the method. We also describe some procedures that can be used to enrich the coarse spaces in order to obtain better approximations if needed.

4.1 Unified definition of coarse basis functions using domain transformations

We introduce a transformation $F^h:\Gamma^h\to\mathbb{R}^3$ and denote by $\widetilde{\Gamma}^h$ the image of the original surface Γ^h under the transformation F^h; that is,

$$\widetilde{\Gamma}^h = F^h(\Gamma^h).$$

We refer to $\widetilde{\Gamma}^h$ as the transformed (or deformed) surface. We use similar notations for the images of fine- and coarse-grid elements, edges and vertices associated to Γ^h; that is, we use $\widetilde{K}_i^h$, $\widetilde{e}_i^h$, $\widetilde{p}_i^h$, $\widetilde{K}_i^H$, $\widetilde{e}_i^H$ and $\widetilde{p}_i^H$. For instance, $\widetilde{K}_i^h = F^h(K_i^h)$.

Multiscale basis functions satisfy the leading order homogeneous equation in each K_i^H and our goal is to construct boundary conditions to compute these multiscale basis functions. The boundary conditions are constructed on the deformed surface $\widetilde{\Gamma}^h$. We construct the boundary condition for the I-th coarse node in the following way. We start with the value at the coarse-grid vertex,

$$\widetilde{b}_I(\widetilde{p}_J^H) = \delta_{IJ}$$

and, on each coarse-grid edge, $\widetilde{b}_I(\cdot)$ will be assumed to satisfy

$$-\Delta_{\widetilde{e}^h}\widetilde{b}_I = 0, \text{ in every edge } \widetilde{e}.$$

Here, $-\Delta_{\widetilde{e}^h}$ is Laplace-Beltrami operator along the edge $\widetilde{e}^h$. Next, for each vertex p_I^H in the original surface Γ^h, we define a multiscale basis function by

$$-\mathrm{div}_s(\kappa\nabla_s\chi_I) = 0 \quad \text{in } K_I^H\subset\omega_I^H, \tag{4.1a}$$

$$\chi_I = \widetilde{b}_I\circ F^h \quad \text{on } \partial K_I^H. \tag{4.1b}$$

See Fig. 5 for an illustration. We introduce the coarse space

$$V_0^{F^h} = \text{span}\{\chi_I\}. \tag{4.2}$$

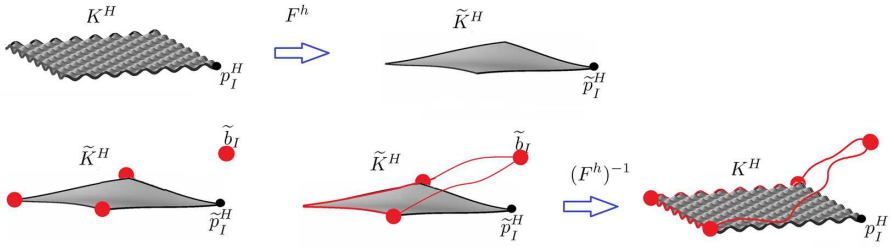

Figure 5: Illustration of the computation of the boundary conditions in the transformed surface to compute basis functions in the original surface.

Remark 4.1. We would like to remark that the MsFEM formulation allows one to take advantage of scale separation. In particular, instead of the coarse element K^H in (4.1), a representative smaller volume can be chosen. See [25] for discussions.

Remark 4.2. Global information can also be incorporated in the construction of multiscale basis functions. See for instance [24,42] where various choices of global information are proposed. Energy minimizing procedures are considered in [47].

Remark 4.3. In the case of open domains, that is Γ being an open subset of $\mathbb{R}^3$, it is well known that, with the use of linear boundary conditions, resonance errors appear. This is due to the fact that the fine-scale solution is, in general, not piecewise linear on the boundary of the coarse-grid elements. In order to overcome resonance errors, different multiscale techniques can be used to impose the boundary conditions of the multiscale basis functions. Many other boundary conditions are introduced and analyzed in the literature. For instance, an *oversampling technique* can be employed (see [32,33]). Another example is the reduced boundary conditions which are found to be efficient in many porous media applications (see [36]).

4.2 Examples of domain deformations

4.2.1 Identity

When $F^h = Id$, where Id is the identity operator in Γ^h, the corresponding coarse space is denoted by $V_0^{Id} = \text{span}\{\chi_I\}$. When Γ^h is an open domain in $\mathbb{R}^2$, the space V_0^{Id} coincides with the multiscale space that uses an auxiliary one-dimensional problem over the edges. See [25].

4.2.2 Harmonic coordinates

We follow metric-based upscaling ideas developed in [42,43] for open subdomains. We extend some of the ideas in [42,43] to problems posed on surfaces. The main idea is to find a domain transformation such that, the oscillatory problem in current coordinates, transforms into a smoother problem in the new coordinates. The change of coordinates

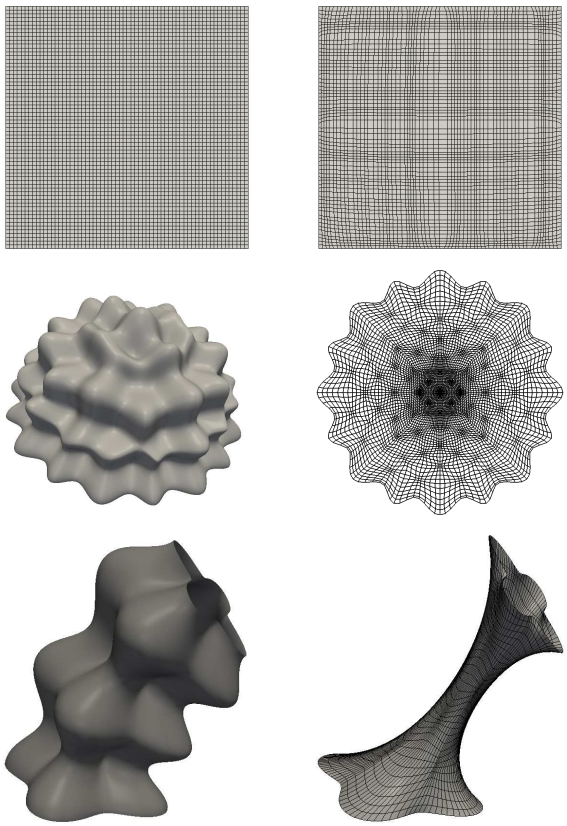

Figure 6: Illustration of harmonic deformations. We show the original domain (on the left) and its image through the harmonic deformation (on the right) for different surfaces. By row: square domain with periodic diffusion coefficient, oscillatory surface over a hemi-sphere and oscillatory bended pipe. Observe that for the first two cases, the deformed domains are on a plane, and for the oscillatory surfaces, the deformed surfaces are "smooth" (without oscillations); this being a typical property of the proposed harmonic map.

is given by $F^h_{Har}:\Gamma\to\mathbb{R}^3$ such that F^h_{Har} is the fine-scale finite element approximation of

$$-\mathrm{div}_S(\kappa\nabla_S F)=0 \quad \text{in } \Gamma \tag{4.3}$$

with one of the following boundary conditions: Dirichlet boundary condition

$$F=\mathrm{Id} \quad \text{on } \partial\Gamma, \tag{4.4}$$

or Neumann boundary condition

$$\kappa\nabla_S F\cdot\boldsymbol{\nu}_S=\boldsymbol{\nu}_S \quad \text{on } \partial\Gamma, \tag{4.5}$$

where $\boldsymbol{\nu}_S$ denotes the co-normal vector. The corresponding coarse space is denoted by $V_0^{F^h_{Har}}=\mathrm{span}\{\chi_I\}$. Fig. 6 illustrates the harmonic deformation obtained for different surfaces.

4.3 Discussion on the convergence

To motivate the proposed harmonic coordinates transformation, consider the case when the boundary curve of the surface lies on a plane. In this case, it is not difficult to show that the image of F^h_{Har} will be the plane region bounded by the curve representing the boundary of the surface.

Using this transformation as a change of variables, one can also show that the surface equation

$$-\mathrm{div}_s(\kappa\nabla_s u) = f \quad \text{in } \Gamma$$

transforms to

$$-\kappa : D^2\hat{u} = \hat{f} \quad \text{in } F^h_{Har}(\Gamma).$$

For example, let us consider the Laplace-Beltrami equation ($\kappa = \boldsymbol{I}$) on different rough surfaces that share the same boundary. In this case, even though F^h_{Har} will be different for the different surfaces, the image $\hat{\Gamma} = F^h_{Har}(\Gamma)$ will be the same for all of them. And, the deformed problem is $-\Delta\hat{u} = \hat{g}$ for each surface. Any roughness of the surface is reduced to appear only on the boundary condition and/or in the source term. Then, assuming that 1) the transformed grid is adequate and 2) the transform boundary condition is smooth, we see that using standard basis on the deformed domain will give the classical finite element error behavior, and thus our MsFEM does not suffer of resonance errors in this case.

Remark 4.4 (Implementation using appropriate grids)**.** It is important to note that, for implementation purposes, it has to be decided the amount of computational time and work dedicated to the construction of coarse-grids. One can construct a grid in the original surface and then map this grid to the deformed surface. One can also construct a coarse-grid on the deformed surface and map it back to the original surface. As suggested by our previous discussions, the latter choice results in no resonance errors. Unfortunately, constructing grids on deformed surfaces is complicated since, in general, only a polyhedral description of the transformed surface is available. For this reason, we will present only numerical examples where we construct coarse-grids only on the original surfaces. This choice does not guarantee the absence of resonance errors (especially for surfaces with complicated boundaries), but it is a more practical choice from the computational point of view. This discrepancy will show as a resonance error in some simulations that would disappear by developing a better way to grid the deformed mesh. We mention that, in Section 4.4, we propose an alternative way to reduce resonance errors without constructing complicated grids that uses local spectral information to *enrich* the coarse spaces constructed with standard grids on the original surfaces. This is a topic where we plan to do further research.

Remark 4.5 (Analitical issues)**.** In the paper, our goal is to propose a computational approach. The analysis of the proposed methods will be studied in future. It is worth mentioning a couple of relevant question in the analytical context. One question is under

what conditions is the solution of the harmonic equation a diffeomorphism and related to this one are the conditions for the finite element approximation to this solution to be one to one. Also, it would be important to analytically quantify how much the oscillations on the deformed surface are reduce through the harmonic transformation. We are currently working on these questions.

4.4 Enrichment using local spectral information for complicated diffusion coefficients

In many cases, e.g., in the presence of high-contrast media properties, one needs to enrich the space to achieve better approximation of the solution. These issues have been studied for equations that are described in $\mathbb{R}^2$ and $\mathbb{R}^3$. In this section, we discuss how initial coarse space, defined as above, can be enriched in a systematic way. See [20, 22, 23] and references therein.

In general, we can consider the basis functions given, as before, by

$$-\mathrm{div}_s(\kappa\nabla_s\chi_I)=0 \quad \text{in } K_I^H\subset\omega_I^H, \tag{4.6a}$$

$$\chi_I=b_I \quad \text{on } \partial\omega_I^H, \tag{4.6b}$$

where the boundary conditions b_I are determined using procedures that involve the transformation of the reference surface. Using these multiscale basis functions, we define a function on the surface (see [20, 22, 23])

$$\widetilde{\kappa}=\sum_I \kappa\nabla_s\chi_I\cdot\nabla_s\chi_I.$$

Using $\widetilde{\kappa}$, we define an eigenvalue problem

$$-\mathrm{div}_s(\kappa\nabla_s\Phi_{I,l})=\lambda_l\widetilde{\kappa}\Phi_{I,l} \quad \text{in } K_I^H\subset\omega_I^H, \tag{4.7a}$$

$$\nabla_s\Phi_{I,l}\cdot\nu=0 \quad \text{on } \partial\omega_I^H. \tag{4.7b}$$

Using dominant eigenvalues (starting with the smallest), we enrich our initial multiscale space that is spanned by χ_I with $\chi_I\Phi_{I,l}$, $l=1,\cdots,L_I$. This leads to a more accurate approximation of the fine-scale solution. In particular, convergence is expected as L_I increases, where L_I is the number of eigenvectors included in the coarse space. The convergence rate is related to the rate of growth of the eigenvalues above. We expect the rate of growth of the eigenvalues to be similar the case of problems posed in open domains where the rate of growth of the eigenvalues and the number of dominant modes are determined by the variations of the coefficient. This and related approaches are shown to be effective when the coefficient varies widely and the problem domain is an open subset of $\mathbb{R}^d$. See [20, 22, 23] and references therein. The results of this procedure and related ones (applied to equations on surfaces) will be reported elsewhere.

5 Numerical simulations

We implemented MsFEM described in Section 4.1 with two domain transformations: (1) the no-deformation (i.e. where the deformation is the identity) of Section 4.2.1 (we call MsFEM-Id) and (2) the harmonic transformation of Section 4.2.2 (we call MsFEM-Hr). At the implementation level, the surface is given by the fine grid; no analytic expression is necessary and no restrictions as far as of its shape or topology are required. Every aspect of the method is developed on the (discrete fine) surface itself. The coarse-grid is formed by an agglomeration of fine cells (see Fig. 4 for illustration). The implementation is coded with the help of the Deal.II library [6], and the figures were generated with Paraview [11].

For the first simulation, we solve a quasiperiodic coefficient elliptic problem on a square (special case of a smooth surface). We consider the oscillatory coefficients given by

$$\kappa_{d,d}=6+\sin\left(\frac{x_d}{\epsilon}\right)+\sin\left(\frac{x_d}{\epsilon\sqrt{5}}\right)+\sin\left(\frac{x_d}{\epsilon\sqrt{10}}\right)+\sin\left(\frac{x_d}{\epsilon\sqrt{20}}\right)+\sin\left(\frac{x_d}{\epsilon\sqrt{50}}\right) \tag{5.1}$$

and take $\epsilon=0.03$. The fine mesh is taken to be a regular Cartesian mesh with the total degrees of freedom of 263169 (this is about 10 points per ϵ in each direction). First, we show some harmonic coordinates in Fig. 7 where we show the deformation of a uniform Cartesian grid in the original domain. We present numerical convergence for varying coarse-mesh size in Table 1. The first column shows the number of total basis functions used in MsFEM and the third column presents the ratio between the coarse-mesh size and ϵ. As in standard MsFEM, we expect to observe a resonance error when H/ϵ is close to unity for MsFEM-Id. This can be observed for both L^2 and H^1 errors from columns 4 and 5. On the other hand, when MsFEM-Hr is employed, we see that there is no resonance error (see Columns 6 and 7 in Table 1) and the method has first-order convergence in the H^1 norm. coefficients.

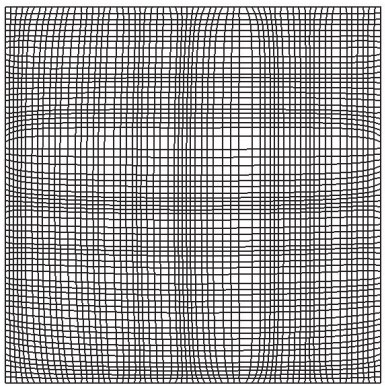

Figure 7: Harmonic deformation (view on a coarser grid) corresponding to the elliptic problem with rough coefficients on the unit square whose convergence behaviour is shown in Table 1.

Table 1: Relative errors for the approximate solution of Eq. (1.1) on the unit square with a diagonal diffusion tensor $\kappa_{d,d}$=6+sin($\frac{x_d}{\epsilon}$)+sin($\frac{x_d}{\epsilon\sqrt{5}}$)+sin($\frac{x_d}{\epsilon\sqrt{10}}$)+sin($\frac{x_d}{\epsilon\sqrt{20}}$)+sin($\frac{x_d}{\epsilon\sqrt{50}}$) and ϵ=0.03, ϵ/h=10.9 and fine problem number of dofs 263169.

# basis	H	H/ϵ	MsFem-Id				MsFem-Hr			
			L^2 error	EOC	H^1 error	EOC	L^2 error	EOC	H^1 error	EOC
9	0.707	23.6	0.320	-	0.567	-	0.332	-	0.581	-
25	0.354	11.8	0.081	2.0	0.287	1.0	0.090	1.9	0.299	1.0
81	0.177	5.9	0.029	1.5	0.179	0.7	0.024	1.9	0.157	0.9
289	0.088	2.9	0.025	0.2	0.162	0.1	0.006	2.0	0.075	1.1
1089	0.044	1.5	0.014	0.8	0.118	0.5	0.002	1.6	0.036	1.1

Next, we consider the Laplace-Beltrami equation on a quasi-periodic rough surface that can be described as a graph over the unit square. More precisely, we consider the graph of $f(x_1,x_2)=\sum_i^3(\epsilon/c_i)(\cos(c_ix_1/\epsilon)+\cos(c_ix_2/\epsilon))$ with (x_1,x_2) in the unit square and $c=(1,\sqrt{5},\sqrt{10})$. In Fig. 8, we depict the original surface (left picture) and the illustration of the harmonic deformation for a coarse block shown with light color on the left plot. In Table 2, we present convergence results for MsFEM-Id and MsFEM-Hr. As before, the number of multiscale basis functions are shown on Column 1. We observe that MsFEM-Id has a resonance error and, in particular, the error does not decrease much as the coarse mesh decreases when H/ϵ is close to unity. On the other hand, MsFEM-Hr has better accuracy compared to MsFEM-Id when H/ϵ is close to unity. As mentioned earlier, the reason for MsFEM-Hr to exhibit a slow convergence rate at $H/\epsilon\approx 1$ is that the coarse mesh in the deformed configuration, that is obtained from the coarse mesh in the

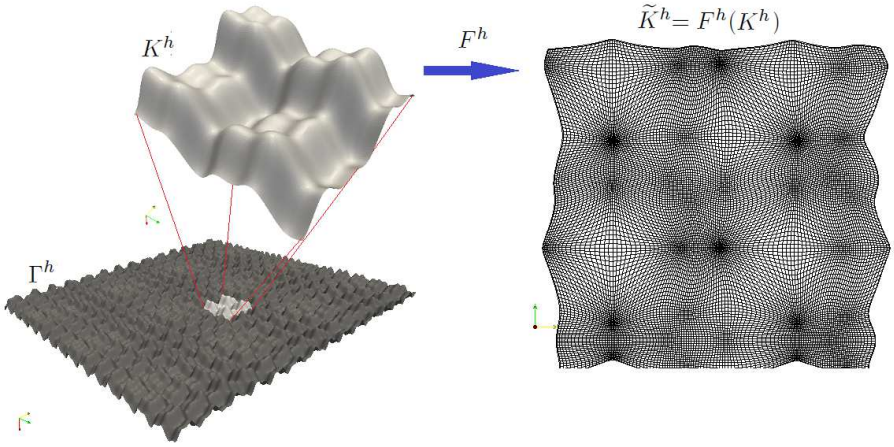

Figure 8: Illustration of the surface obtained as quasi-periodic perturbation of a plane and the harmonic deformation F_{Har}. Bottom left: actual surface where the problem is posed and solved. Top right: zoom out of a the grayed piece of the surface. Bottom right: piece of the deformed domain corresponding to the image by F_{Har} of the grayed piece of surface. Convergence behavior for the elliptic problem on this surface is shown in Table 2.

Table 2: Relative errors for the approximate solution of Eq. (1.1) on a surface that oscillates about a square with an identity diffusion tensor. The surface is generated as $(x_1,x_2,\sum_i^3(\epsilon/c_i)(\cos(c_ix_1/\epsilon)+\cos(c_ix_2/\epsilon))$ with (x_1,x_2) in the unit square, $\boldsymbol{c}=(1,\sqrt{5},\sqrt{10})$ and $\epsilon=0.005$, $\epsilon/h=7.6$ and fine problem number of dofs 1050625.

# basis	H	H/ϵ	MsFem-Id				MsFem-Hr			
			L^2 error	EOC	H^1 error	EOC	L^2 error	EOC	H^1 error	EOC
9	0.707	22.5	0.332	-	0.580	-	0.329	-	0.577	-
25	0.356	11.3	0.095	1.8	0.312	0.9	0.091	1.9	0.301	0.9
81	0.179	5.7	0.036	1.4	0.196	0.7	0.028	1.7	0.170	0.8
289	0.090	2.9	0.039	-0.1	0.195	0.0	0.020	0.5	0.140	0.3
1089	0.062	2.0	0.049	-0.3	0.221	-0.2	0.021	-0.1	0.144	0.0
4225	0.053	1.7	0.038	0.4	0.195	0.2	0.009	1.2	0.095	0.6
16641	0.031	1.0	0.017	1.2	0.129	0.6	0.005	0.8	0.069	0.5

reference configuration by our harmonic map, is not regular and thus we do not have a standard convergence in the deformed configuration.

For the third example, we consider an oscillatory surface that is obtained by perturbing a semi-sphere with a quasiperiodic function. This perturbation is obtained in the following way. First, we select a few points on the sphere (in this case 12 points quasi-equidistributed) and consider the tangent planes through these points. Over each tangent plane we consider the function $\epsilon(\cos(x_1/\epsilon)+\cos(x_2/\epsilon))$, where x_1 and x_2 are the local plane coordinates. This function defined on each plane is then projected to the sphere and gives the particular plane contribution to the amplitude of the normal pertur-

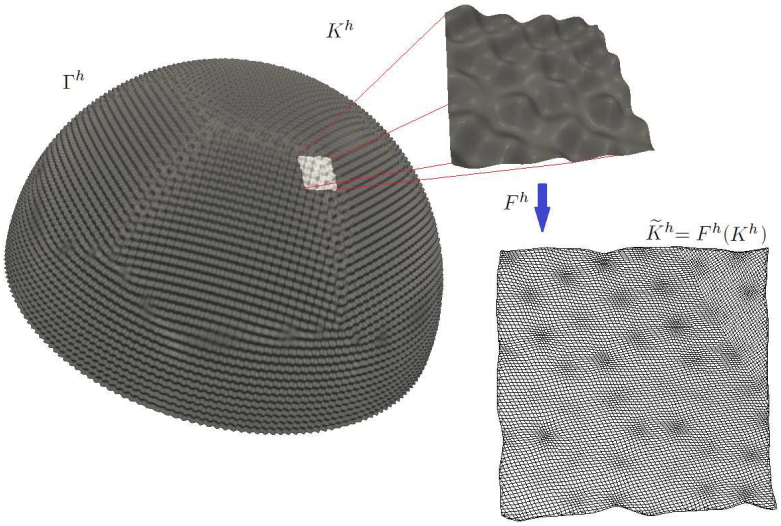

Figure 9: Illustration of the surface obtained as normal perturbation of a semisphere and the harmonic deformation F_{Har}. Left: actual surface where the problem is posed and solved. Top right: zoom out of a the grayed piece of the surface. Bottom right: piece of the deformed domain corresponding to the image by F_{Har} of the grayed piece of surface. Convergence behavior for the elliptic problem on this surface is shown in Table 3.

Table 3: Relative errors for the approximate solution of Eq. (1.1) on an oscillatory surface around a half sphere with an identity diffusion tensor. Here, $\epsilon=0.005$, $\epsilon/h=4.6$ and fine problem number of dofs 1311745.

# basis	H	H/ϵ	MsFem-Id				MsFem-Hr			
			L^2 error	EOC	H^1 error	EOC	L^2 error	EOC	H^1 error	EOC
25	0.947	30.1	0.041	-	0.192	-	0.034	-	0.176	-
89	0.504	16.0	0.011	1.9	0.099	1.0	0.009	1.9	0.090	1.0
337	0.257	8.2	0.004	1.5	0.058	0.8	0.003	1.6	0.049	0.9
1313	0.129	4.1	0.003	0.4	0.052	0.2	0.002	0.6	0.036	0.4
5185	0.066	2.1	0.005	-0.7	0.065	-0.3	0.002	0.0	0.042	-0.2
20609	0.035	1.1	0.008	-0.7	0.080	-0.3	0.003	-0.6	0.045	-0.1
82177	0.023	0.7	0.004	1.0	0.052	0.6	0.001	1.6	0.030	0.6

Table 4: Relative errors for the approximate solution of Eq. (1.1) on an oscillatory surface around a torus section with an identity diffusion tensor. Here, $\epsilon=0.05$, $\epsilon/h=8.4$ and the fine problem has the number of dofs 787968.

# basis	H	H/ϵ	MsFem-Id				MsFem-Hr			
			L^2 error	EOC	H^1 error	EOC	L^2 error	EOC	H^1 error	EOC
18	0.518	16.5	0.239	-	0.487	-	0.184	-	0.422	-
60	0.278	8.9	0.064	1.9	0.252	1.0	0.047	2.0	0.209	1.0
216	0.142	4.5	0.023	1.5	0.153	0.7	0.015	1.6	0.117	0.8
816	0.073	2.3	0.020	0.2	0.141	0.1	0.008	0.9	0.087	0.4
3168	0.039	1.2	0.033	-0.7	0.182	-0.4	0.008	0.0	0.086	0.0

bation on the sphere. More precisely, we set a cut-off radius (in this case 0.7) for all the planes and we blend the contribution of each with a partition of unity over the sphere. We then solve the Laplace-Beltrami equation with the right-hand-side $f=1$ and homogeneous boundary conditions. In Fig. 9, we depict the original oscillatory sphere and a coarse region (left picture) and the transformation of this coarse region (right figure). Numerical results are presented in Table 3. As we observe from this table, MsFEM-Hr has a better accuracy compared to MsFEM-Id and a better convergence rate. However, we observe the resonance error in MsFEM-Hr due to the gridding issue discussed earlier.

For our last numerical example, we study MsFEM-Id and MsFEM-Hr for the Laplace-Beltrami equation on an oscillating torus, see Fig. 10 (left picture). In this case, a sectional piece of torus is normally perturbed by $\epsilon(\cos(\theta/\epsilon)+\cos(\phi/\epsilon))$, where θ and ϕ are the angles of the major and minor circles corresponding to the point. The Laplace-Beltrami equation is solved with the source term $f=1$ and homogeneous Dirichlet boundary conditions. Numerical results are presented in Table 4 for varying coarse-mesh size and fixed ϵ. In Fig. 5, we plot these errors against the coarse-mesh size. As we observe from these numerical results, MsFEM-Hr converges faster and the error for decreasing H reduces faster for MSFEM-Hr compared to MsFEM-Id. These results show that MsFEM-Hr has smaller resonance effects though, as we discussed it, still contains resonance errors due to coarse-grid ding.

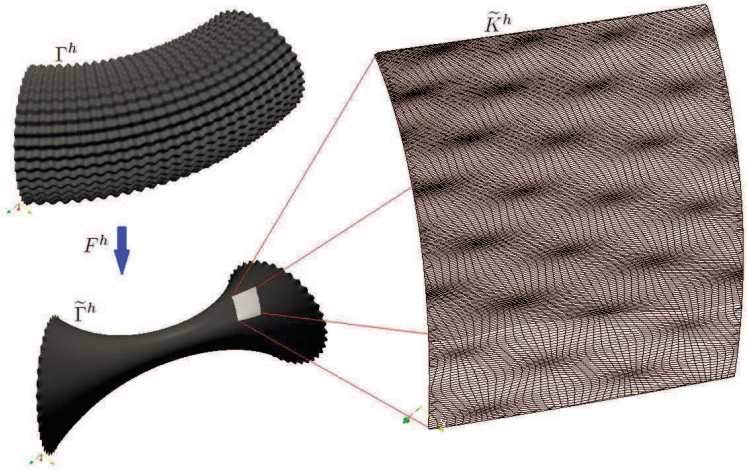

Figure 10: Oscillating toroidal section surface and its harmonic deformation. Top left: actual surface where the problem is posed and solved. Bottom left: Deformed surface. Right: piece of the deformed domain corresponding to the image by F_{Har} of the grayed piece of surface. Convergence behavior for the elliptic problem on this surface is shown in Table 4.

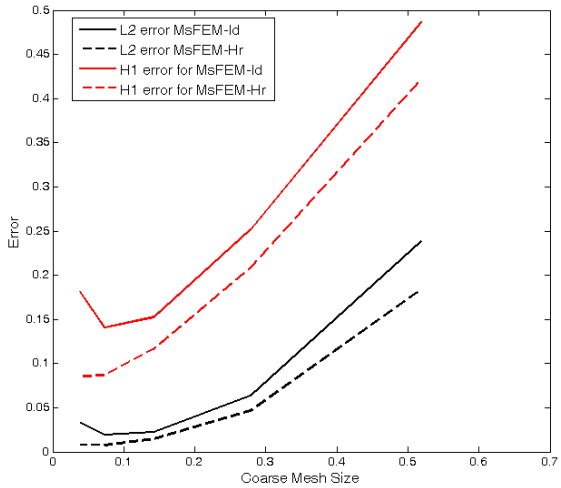

Figure 11: Error comparisons between MsFEM-Id and MsFEM-Hr. Solid lines designate MsFEM-Id error (red lines are for H^1 errors and black lines for L^2 errors) and dashed lines represent the errors for MsFEM-Hr.

6 Conclusions

In this paper, we develop multiscale finite element methods (MsFEMs) for problems on rough surfaces. The proposed approach consists of two parts: (1) multiscale basis function computations; (2) coupling multiscale basis functions in a global variational formulation. We consider the diffusion problem, though the proposed concepts can be applied to more general equations. The multiscale basis computation entails the use of transforma-

tions that map the reference surface to the deformed surface. On the deformed surface, the computation of basis functions is defined and then these basis functions are used in the reference domain. In particular, reduced (1D) problems are solved along the edges of coarse-grid blocks to calculate nodal multiscale basis functions in the deformed domain. We discuss the use of appropriate transformation operators that improve the accuracy of the method. The method has an optimal convergence if the transformed surface is smooth and the image of the coarse partition in the reference configuration forms a quasiuniform partition. Numerical results are presented where we compare two different multiscale basis functions: (1) basis functions that are computed using local deformations; (2) basis functions that are computed using global deformations. Our numerical results show that the second approach is more accurate and we discuss the convergence of the method.

Acknowledgments

YE's work is partially supported by the US Army 62151-MA, DOE and NSF (DMS 0934837, DMS 0724704, and DMS 0811180). This publication is based in part on work supported by Award No. KUS-C1-016-04, made by King Abdullah University of Science and Technology (KAUST).

References

[1] J. E. Aarnes, On the use of a mixed multiscale finite element method for greater flexibility and increased speed or improved accuracy in reservoir simulation, SIAM Multiscale Model. Simul., 2 (2004), 421-439.
[2] J. E. Aarnes, Y. Efendiev, and L. Jiang, Mixed multiscale finite element methods using limited global information, SIAM Multiscale Model. Simul., 7(2) (2008), 655-676.
[3] A. Abdulle and C. Schwab, Heterogeneous multiscale FEM for diffusion problems on rough surfaces, Multiscale Model. Simul., 3(1) (2004/05), 195-220 (electronic).
[4] T. Aubin, Nonlinear Analysis on Manifolds. Monge-Ampère Equations, volume 252 of Grundlehren der Mathematischen Wissenschaften [Fundamental Principles of Mathematical Sciences]. Springer-Verlag, New York, 1982.
[5] I. Babuška, V. Nistor, and N. Tarfulea, Generalized finite element method for second-order elliptic operators with Dirichlet boundary conditions, J. Comput. Appl. Math., 218(1) (2008), 175-183.
[6] W. Bangerth, R. Hartmann, and G. Kanschat, deal.II – a general purpose object oriented finite element library, ACM Trans. Math. Softw., 33(4) (2007), 24/1–24/27.
[7] A. Bensoussan, J. L. Lions, and G. Papanicolaou, Asymptotic analysis for periodic structures, volume 5 of Studies in Mathematics and Its Applications. North-Holland Publ., 1978.
[8] L. Berlyand and H. Owhadi, A new approach to homogenization with arbitrary rough high contrast coeffcients for scalar and vectorial problems, arXiv:0901.1463v3.
[9] L. Berlyand and H. Owhadi, Flux norm approach to finite dimensional homogenization approximations with non-separated scales and high contrast, Arch. Ration. Mech. Anal., 198(2) (2010), 677-721.

[10] V. Calo, Y. Efendiev, and J. Galvis, A note on variational multiscale methods for high-contrast heterogeneous flows with rough source terms, Adv. Water Resour., 34(9) (2011), 1177V1185.
[11] ParaView, http://www.paraview.org, 2012.
[12] C. C. Chu, I. G. Graham, and T. Y. Hou, A new multiscale finite element method for high-contrast elliptic interface problem, Math. Comp., 79 (2010), 1915-1955.
[13] E. Chung and Y. Efendiev, Reduced-contrast approximations for high-contrast multiscale flow problems, SIAM Multiscale Model. Simul., 8(4) (2010), 1128-1153.
[14] M. C. Delfour and J.-P. Zolésio, Shapes and Geometries: Analysis, Differential Calculus, and Optimization, volume 4 of Advances in Design and Control. Society for Industrial and Applied Mathematics (SIAM), Philadelphia, PA, 2001.
[15] U. Dierkes, S. Hildebrandt, A. Küster, and O. Wohlrab, Minimal Surfaces, I - Introduction and Boundary Value Problems, volume 295 of Grundlehren der Mathematischen Wissenschaften [Fundamental Principles of Mathematical Sciences]. Springer-Verlag, Berlin, 1992.
[16] L. J. Durlofsky, Coarse scale models of two-phase flow in heterogeneous reservoirs: Volume averaged equations and their relation to existing upscaling techniques, Comp. Geosciences, 2 (1998), 73-92.
[17] L. J. Durlofsky, Y. Efendiev, and V. Ginting, An adaptive local-global multiscale finite volume element method for two-phase flow simulations, Adv. Water Resour., 30 (2007), 576-588.
[18] G. Dziuk, Finite elements for the Beltrami operator on arbitrary surfaces, in Partial Differential Equations and Calculus of Variations, volume 1357 of Lecture Notes in Math.. Springer, Berlin, 1988, pages 142–155.
[19] J. Eberhard, S. Attinger, and G. Wittum, Coarse graining for upscaling of flow in heterogeneous porous media, SIAM Multiscale Model. Simul., 2(2) (2004), 269-301.
[20] Y. Efendiev and J. Galvis, A domain decomposition preconditioner for multiscale high-contrast problems, in Domain Decomposition Methods in Science and Engineering XIX, Y. Huang, R. Kornhuber, O. Widlund, and J. Xu (Eds.), volume 78 of Lecture Notes in Computational Science and Engineering. Springer-Verlag, 2011, Part 2, pages 189-196.
[21] Y. Efendiev, J. Galvis and P. Vassielvski, Spectral element agglomerate algebraic multigrid methods for elliptic problems with high-Contrast coefficients, in Domain Decomposition Methods in Science and Engineering XIX, Y. Huang, R. Kornhuber, O. Widlund, and J. Xu (Eds.), volume 78 of Lecture Notes in Computational Science and Engineering. Springer-Verlag, 2011, Part 3, pages 407-414.
[22] Y. Efendiev, J. Galvis, R. Lazarov and J. Willems, Robust domain decomposition preconditioners for abstract symmetric positive definite bilinear forms, ESAIM: Math. Model. Numer. Anal., 46 (2012), 1175-1199.
[23] Y. Efendiev, J. Galvis, and X. H. Wu, Multiscale finite element methods for high-contrast problems using local spectral basis functions, J. Comput. Phys., 230(4) (2011), 937-955.
[24] Y. Efendiev, V. Ginting, T. Hou, and R. Ewing, Accurate multiscale finite element methods for two-phase flow simulations, J. Comput. Phys., 220(1) (2006), 155-174.
[25] Y. Efendiev and T. Hou, Multiscale Finite Element Methods. Theory and Applications. Springer, 2009.
[26] Y. Efendiev, T. Hou, and V. Ginting, Multiscale finite element methods for nonlinear problems and their applications, Comm. Math. Sci., 2 (2004), 553-589.
[27] Y. Efendiev, T. Y. Hou, and X. H. Wu, Convergence of a nonconforming multiscale finite element method, SIAM J. Num. Anal., 37 (2000), 888-910.
[28] W. E and B. Engquist, The heterogeneous multiscale methods, Commun. Math. Sci., 1(1)

(2003), 87-132.
[29] D. Gilbarg and N. S. Trudinger, Elliptic partial differential equations of second order, volume 224 of Grundlehren der Mathematischen Wissenschaften [Fundamental Principles of Mathematical Sciences]. Springer-Verlag, Berlin, second edition, 1983.
[30] A. Gloria, Analytical framework for the numerical homogenization of elliptic monotone operators and quasiconvex energies, SIAM Multiscale Model. Simul., 5(3) (2006), 996-1043.
[31] A. Gloria, Reduction of the resonance error. Part 1: Approximation of homogenized coefficients, Math. Models Methods Appl. Sci. (M3AS), 1 (2011), 1-30. DOI: 10.1142/S0218202511005507.
[32] T. Y. Hou and X. H. Wu, A multiscale finite element method for elliptic problems in composite materials and porous media, J. Comput. Phys., 134 (1997), 169-189.
[33] T. Y. Hou, X. H. Wu, and Z. Cai, Convergence of a multiscale finite element method for elliptic problems with rapidly oscillating coefficients, Math. Comp., 68 (1999), 913-943.
[34] T. Y. Hou, X. H. Wu, and Y. Zhang, Removing the cell resonance error in the multiscale finite element method via a Petrov-Galerkin formulation, Commun. Math. Sci., 2(2) (2004), 185-205.
[35] T. Hughes, G. Feijoo, L. Mazzei, and J. Quincy, The variational multiscale method - a paradigm for computational mechanics, Comput. Methods Appl. Mech. Engrg, 166 (1998), 3-24.
[36] P. Jenny, S. H. Lee, and H. Tchelepi, Multi-scale finite volume method for elliptic problems in subsurface flow simulation, J. Comput. Phys., 187 (2003), 47-67.
[37] I. Lunati and P. Jenny, Multiscale finite-volume method for compressible multiphase flow in porous media, J. Comput. Phys., 216 (2006), 616-636.
[38] I. Lunati and P. Jenny, The Multiscale Finite Volume Method: A flexible tool to model physically complex flow in porous media, in: Proceedings of European Conference of Mathematics of Oil Recovery X, Amsterdam, The Netherlands, September 4-7, 2006.
[39] A. L. Madureira, A multiscale finite element method for partial differential equations posed in domains with rough boundaries, Math. Comp., 78(265) (2009), 25-34.
[40] J. Nolen, G. Papanicolaou, and O. Pironneau, A framework for adaptive multiscale method for elliptic problems, SIAM Multiscale Model. Simul., 7 (2008), 171-196.
[41] M. Ohlberger, A posterior error estimates for the heterogenoeous mulitscale finite element method for elliptic homogenization problems, SIAM Multiscale Model. Simul., 4(1) (2005), 88-114.
[42] H. Owhadi and L. Zhang, Metric based up-scaling, Comm. Pure Appl. Math., 60(5) (2007), 675-723.
[43] H. Owhadi and L. Zhang, Localized bases for finite dimensional homogenization approximations with non-separated scales and high-contrast, Caltech ACM Tech Report No 2010-04, arXiv:1011.0986.
[44] J. Sokołowski and J.-P. Zolésio, Introduction to Shape Optimization: Shape Sensitivity Analysis, volume 16 of Springer Series in Computational Mathematics. Springer-Verlag, Berlin, 1992.
[45] J. Wloka, Partial Differential Equations, Cambridge University Press, Cambridge, 1987. Translated from the German by C. B. Thomas and M. J. Thomas.
[46] X. H. Wu, Y. Efendiev, and T. Y. Hou, Analysis of upscaling absolute permeability, Discret. Contin. Dyn. Sys. Series B, 2 (2002), 185-204.
[47] J. Xu and L. Zikatanov, On an energy minimizing basis for algebraic multigrid methods, Comput. Visual Sci., 7 (2004), 121-127.